

Numerical and experimental study of the Ti6Al4V macrostructure obtained by Nd:YAG laser

J. C. Conde · M. D. Paz · J. Serra ·
P. González

Received: 27 March 2013 / Accepted: 9 July 2013 / Published online: 23 July 2013
© Springer-Verlag Berlin Heidelberg 2013

Abstract Titanium and its alloys (Ti6Al4V) have been widely used in the biomedical field; nevertheless, they should be subject to specific surface treatments, before being implanted, in order to improve bio-integration. Although laser processing is a useful technique for this purpose, different aspects of the basic mechanisms of this process are still in progress, with special emphasis on the modeling structure formation on the irradiated surface. For this research, the finite element method was used to study the generation of a macrostructure on the Ti6Al4V surface using a Nd:YAG laser. The temperature profiles, estimated during the extremely high heating and cooling rates caused by the output power of the laser beam, allowed us to analyze, among other things, the melting depth and the heat affected zone, in order to optimize the process. Moreover, the experimental results (SEM data) were positively compared with the numerical model, and a relationship of the crater profile formation (depth to width ratio) was determined.

1 Introduction

The widespread use of titanium (Ti) and its alloys (mainly the aluminum and vanadium alloy, Ti6Al4V) in the biomedical field fulfills many of the requirements of implantology: biocompatibility and osseointegration, biofunctionality (adequate mechanical properties), corrosion resistance, processability and availability. Nowadays, together with

stainless steels and cobalt-chromium alloys, they are used to produce dental, maxillofacial, orthopedic, cardiac, cardiovascular and otorhinolaryngological implants [1, 2].

It is interesting to note that, in many cases, the production of the implant causes surface modifications as a result of the processes of laminating, machining, casting or forging. These changes do not occur evenly over all the material. Under these conditions, the surface is not suitable for medical applications, especially when there is direct contact with the implant tissue. That is why it is necessary to apply surface treatments in order to achieve a uniform finish. Furthermore, in most cases, it is necessary to apply surface treatments to generate specific properties which optimize the function of the medical device in question by obtaining a functional surface. Thus, the surface modification of an implant is defined as the process of changing the properties that appear naturally in the material by rendering them more desirable for implantation. This modification may consist in changing the hydrophobic surface to hydrophilic material in order to create a more biocompatible surface for a medical device. Surface modification is an extremely broad term that includes both methods for performing chemical changes on biomaterials (such as coatings or oxide growth) and methods for modifying the surface topography (in the case of texturing or sanding) [2–5].

The topography can be defined as the set of natural or artificial specific geometric features of a surface. In biomaterials, it is important to consider two basic topographic features, namely texture and roughness. The former encompasses the natural or deliberately arranged configurations of the surface (for example, pores, grooves, valleys, hills or patterns). There is a wide range of techniques to achieve this [6]. In recent years, the laser processing of surfaces for biomedical applications has grown in

J. C. Conde (✉) · M. D. Paz · J. Serra · P. González
Applied Physics Department, University of Vigo,
E.T.S.I. Campus Universitario,
Rúa Maxwell s/n, 36310 Vigo, Spain
e-mail: jconde@uvigo.es

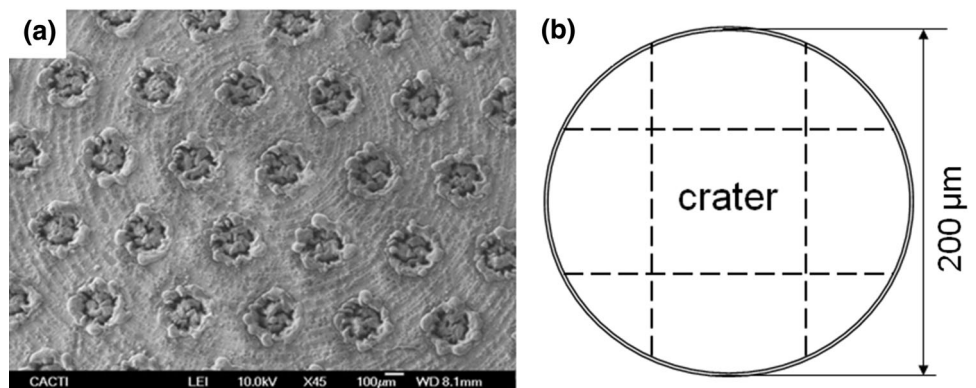
importance [7, 8]. Although laser processing is a useful technique for this purpose, different aspects of the basic mechanisms of this process are still in progress, with special emphasis on the modeling structure formation on the irradiated surface.

The macrostructure generation with lasers on the Ti6Al4V surface requires the application and absorption of high energy densities during a very short interaction time (nanoseconds range), and involves many complex physical phenomena in the material such as electronic, chemical and/or thermal processes. The thermal effects play the main role heating the material, and it can be expressed mathematically by the heat conduction differential equation (HCDE) [9–13]; thus, the numerical methods are a valuable tool for the optimization of surface topographic modifications, since it provides the temperature field and it allowed us the fine-tuning of the experimental conditions, among other things, the maximum melting depth (MMD), maximum boiling depth (MBD) and the HAZ, in order to optimize the process.

2 Experimental procedure

Samples consisted of Ti6Al4V disks 6 mm in diameter and 2 mm thick. The surface was macro structured using an RSM 20E Nd:YAG marking laser ($\lambda = 1,064$ nm, $\tau = 10$ ns, 20 kHz, $\Phi = 6.19$ J cm⁻², spot beam diameter of 60 μ m). These parameters were chosen based on previous studies by other authors [14–16]. The irradiation took place under atmospheric pressure with normal beam incidence without focusing lens. Scanning electron microscopy (JEOL JSM-6700 f) was used to study the macrostructure, as is presented in Fig. 1a. Figure 1b presents the irradiation pattern for each crater; 200 μ m in length was irradiated in both x and y direction with 10 mm/s processing speed, involving 400 laser pulses for each direction.

Fig. 1 **a** SEM micrograph of the macrostructure consisting of a regular pattern of craters; and **b** irradiation pattern used on each crater consisting of two perpendicular series of laser lines inside the circle



3 Numerical simulation

The superficial modification and the thermal distribution induced by the laser irradiation are approached with FEM by using the ANSYS® (13.0) code [17–20] and by solving the HCDE as follows:

$$\begin{aligned} \rho(T)C(T)\partial T(\mathbf{r},t)/\partial t &= \nabla[k(T)\nabla T(\mathbf{r},t)] \quad \text{for } T_o \leq T < T_m \\ \partial H(T)/\partial t &= \nabla[k(T)\nabla T(\mathbf{r},t)] \quad \text{for } T \geq T_m \end{aligned} \quad (1)$$

The model contemplates the dependence of the temperature on the thermal properties of the Ti6Al4V: the density ρ (g/cm³), the thermal conductivity k (W/cm²K) and the specific heat C (J/gK) [21–27]. The phase changes are considered by the enthalpy H (J/cm³):

$$H(T) = \int_{T_o}^T \underbrace{\rho(T')C(T')dT'}_{\text{if } T_o \leq T < T_m} + \underbrace{h(T - T_m)L_m}_{\text{if } T_m \leq T < T_b} + \underbrace{h(T - T_b)L_v}_{\text{if } T \geq T_b} \quad (2)$$

where h is the Heaviside function, the $T_{m/b}$ (K) are the melting/boiling temperatures and $L_{m/v}$ (J/g) is the melting/evaporation heat. As boundary conditions, the initial temperature, $T(\mathbf{r}, 0) = 300$ K, is considered in the whole volume, and the heat flux impinges in the normal direction to the target surface.

This heat flux provided by the laser source is defined by the initial beam intensity $I(\mathbf{r}, t)$ which incorporates the main laser beam parameters as the energy density F (J/cm²) with a Gaussian-like distribution and the pulse length τ (ns); the optical parameters are also included:

$$\begin{aligned} I(\mathbf{r}, t) &= A(\theta_i)\Phi[F, f(\tau)] \exp\left[-2r/(2^{0.5}S)^2\right] \\ &\times \exp\left[-\varepsilon L\left(1 - (1 - \delta)^{1+\pi/(4\phi)}\right)\right] \end{aligned} \quad (3)$$

where $A = 1 - R(\theta_i, n, \kappa)$ is the absorptivity, $R(\theta_i, n, \kappa)$ is the reflectivity [21, 28], θ_i is the laser beam incidence angle

and n , κ are the components of the complex refraction index; $f(\tau)$ is a pulse length dependent function, r is the radial coordinate, S is the radius of the laser spot, δ is the absorption coefficient of the Ti6Al4V target and ϕ is the average angle between the crater and the initial incident beam axis. Other parameters are related to the first stages of the laser ablation process. As is well known, when the target material reaches the vaporization temperature, particles have been observed to leave the surface by generating a hot plasma cloud (plume) [28], which is visible in the majority of the processes. In the present case, as evidenced in the SEM micrograph (Fig. 1), the laser interaction with the surface produced a crater, resulting from the ablation of the Ti6Al4 V. Thus, the energy density absorbed on the crater wall is also taken into account by means of the plasma absorption during the multiple reflections [29]. The fraction of the energy density which is absorbed when the beam crosses a length in the plasma is given by the Beer-Lambert law: $1 - e^{-\epsilon L}$; where ϵ , is the plasma attenuation coefficient and L is the average path of the laser beam into the plasma before it reaches the crater wall. Authors have reported different ϵ values, i.e., the inverse Bremsstrahlung mechanism is used for CO₂ laser melting, and the average ϵ value is 100 m^{-1} [30]; for the Nd:YAG laser attenuation, the Rayleigh scattering mechanism was applied [31], and an attenuation coefficient of 7 m^{-1} was reported [32]. Due to the multiple reflections that occur inside the crater, the laser beam is absorbed by the plasma. Thus, attenuation in the plasma over the melted surface and attenuation due to the multiple reflections have been taken into account in this

study, and a value of 100 m^{-1} was considered for the calculations. The calculations incorporate the average number of reflections before the appearance of the crater, giving the $1 + (\pi/4\phi)$ parameter (Eq. 3) a value of 6 [29].

4 Results and discussion

The numerical analyses were carried out under the same conditions as the experimental procedure. The laser supplied 2 pulses/ μm in both x - and y -directions, investing a time of $\sim 5 \times 10^4 \text{ ns}$ between two consecutive pulses. This means a very high overlapping degree on a single spot area in both directions, as depicted in Fig. 2a. As shown in Fig. 2b, around 360 laser pulses, from $x = 0 \mu\text{m}$ to $x = 180 \mu\text{m}$, cover the whole irradiated area (the same was applied to the y -coordinate). The simulations were carried out covering $5 \mu\text{m}$, as presented in Table 1. As the room temperature is reached between two consecutive pulses during the cooling, all simulations were conducted using the initial temperature $T(r,0)$.

The hypothesis to implement this numerical model incorporated the main physical changes caused by the temperature gradient. Thus, as is well known, the solid phase of titanium presents different structures: the α -phase appears below 1,158 K and, as the temperature increases, the titanium structure changes to the β -phase. These structural modifications were also added to our hypothesis; these are the transition temperatures, when the $\alpha + \beta$ structure changes to β structure ($TT = 1,220 \text{ K}$), as well as

Fig. 2 **a** Representative scheme of a very high overlapping degree on a single spot area in both directions; **b** On the total irradiated area, it is possible to observe that with four laser pulses, with the spot center located in $x = 0, 60, 120$ and $180 \mu\text{m}$, it would be enough to cover an area of $200 \mu\text{m}$ in diameter; and **c** Hypothesis to implement the numerical model. The estimated parameters are the following: the maximum surface width for the MP and for the TT (ΔMP and ΔTT , respectively) and the HAZ in its liquid phase and the β -phase (*solid*) (HAZ-MP and HAZ-TT, respectively). Below the HAZ-TT is the $\alpha + \beta$ -phase (*solid*) and, finally, the crater depth (CD) and the crater width (CW)

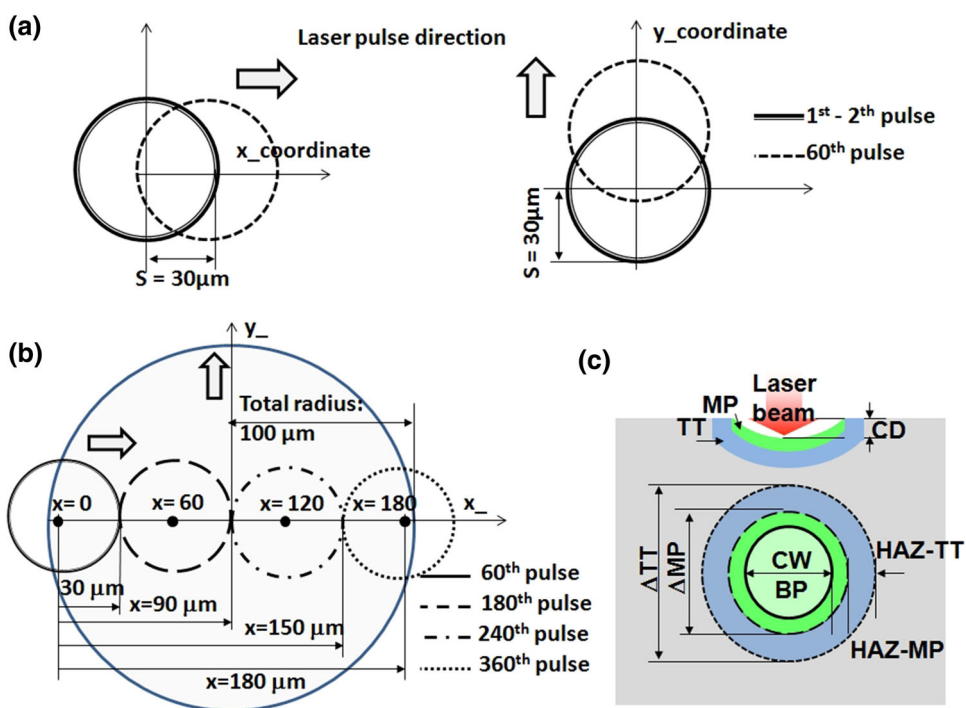


Table 1 Position respect to the initial spot center ($x = 0, y = 0$), the corresponding number of pulses and the key (P_i) used for the first eleven consecutive pulses of the numerical simulation

x (μm)	0	0.5	1.0	1.5	2.0	2.5	3.0	3.5	4.0	4.5	5.0
Pulse	1	2	3	4	5	6	7	8	9	10	11
Key	P1	P2	P3	P4	P5	P6	P7	P8	P9	P10	P11

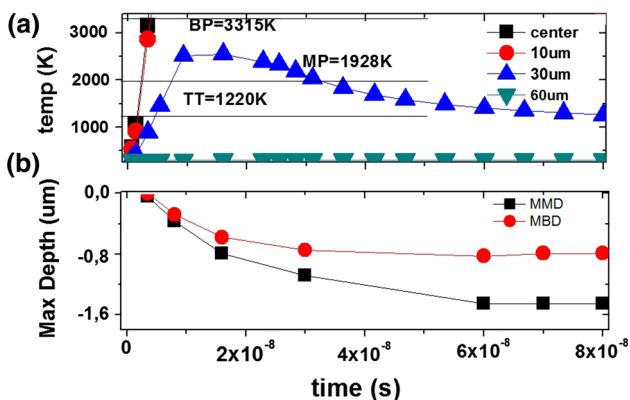


Fig. 3 **a** Evolution of the temperature on the surface as a function of the time, for the initial spot center (P1) and at different distances from P1; **b** isotherms of the MMD and MBD versus time for P1

the melting point ($MP = 1,928 \text{ K}$) and the boiling point ($BP = 3,315 \text{ K}$) [26], which induces changes on the Ti6Al4V structure, as presented in Fig. 2c. So those elements that reached the BP during the laser processing were converted into null elements; thus, they did not participate in the ablation process, and therefore, the crater depth (CD) and its crater width (CW) could be estimated.

The evolution of the temperature on the surface (at different distances from the spot center) versus time is shown in Fig. 3a. We can see that the MP was quickly reached ($\sim 1.5 \text{ ns}$) in the spot center, and the whole spot area was melted at around 30 ns. The BP was also quickly reached 3.5 ns but the spot area was only partially evaporated ($55 \mu\text{m}$), so it was not fully affected. Figure 3b depicts the MMD and the MBD versus time, for the first pulse (P1); we can see the melting and boiling depths were reached at around 0.8 and 1.5 μm , respectively. These results and the observed HAZ profile parameters (see Fig. 2c) are summarized in Fig. 4a. The evolution of the CD/CW follows an exponential behavior as a function of the position (x) from the initial spot distance to the spot center (or number of pulses) as is shown in Fig. 4b. In this way, it was observed that during the first pulses, the crater in the spot center grew very quickly, but the HAZ on the surface seemed to be constant. Thus, the formation of a crater with conical cross section would be possible, as the number of laser pulses increases.

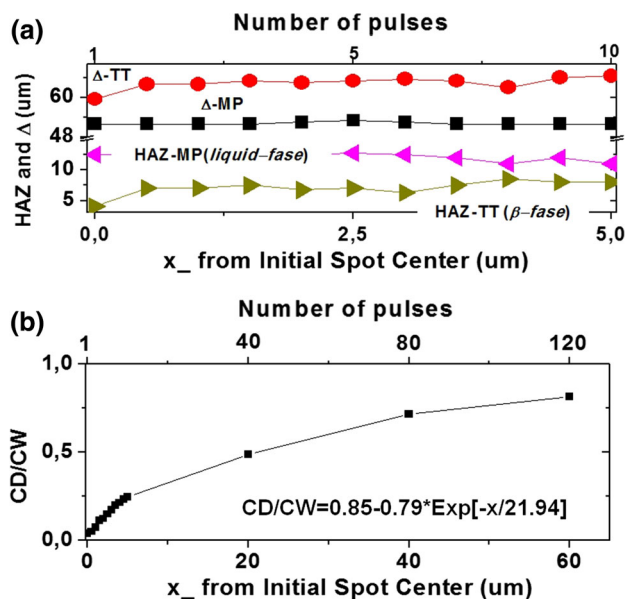


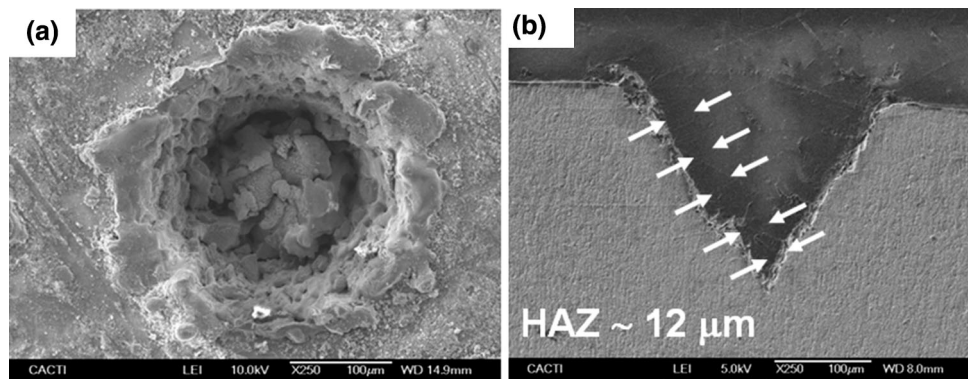
Fig. 4 **a** The parameters ΔMP , ΔTT , the HAZ-MP and the HAZ-TT as a function of the initial spot position for the first eleven consecutive laser pulses at the time where the crater on the spot center is greater [60 ns, for the P1...P11 consecutive laser pulses (Table 1)]; **b** Crater Depth/Crater Width ratio (CD/CW) as a function of the distance from the initial spot center for P1–P11 and for 40, 80 and 120 laser pulses; the evolution can be expressed by an exponential equation

These findings were compared to the experimental data on the laser processing of Ti6Al4V disks (6 mm in diameter and 2 mm thick) carried out under the same conditions as the numerical analysis. Figure 5 shows SEM micrographs of a typical crater formed after 320 laser pulses. The experimental results allowed us to appreciate where the superficial modifications appear in a temperature range between the TT and the MP and also the cavity that clearly appears (SPOT) on the interaction zone when the boiling point is reached. A preliminary quantification can be performed using these micrographs, assuming that the $CD = 190 \mu\text{m}$ and the $CD/CW = 0.844$, based on data obtained after 320 laser pulses. Thus, by using the equations obtained in Fig. 4, for $CD = 190 \mu\text{m}$, we find that the spot center is located at around $x = 164 \mu\text{m}$, which gives 328 laser pulses. For this number of laser pulses, we obtain a $CD/CW = 0.847$, which agrees with the numerical estimations. The estimated HAZ-MP zone, around 12 μm , is clearly visible and concurs with the experimental details (Figs. 4a, 5b).

5 Conclusions

The calculations of the temperature distribution induced by the Nd:YAG during the macro structuration of the Ti6Al4V surface proved to be a very useful tool for the optimization

Fig. 5 SEM micrographs of the crater **a** surface view; and **b** section profile, after 320 laser pulses



of the experimental process parameters. It was demonstrated that the aspect ratio (CD/CW profile) follows an exponential behavior. The numerical model is in agreement with the experimental results obtained in similar conditions.

Acknowledgments This work was partially supported by EU FP7/REGPOT (Grant No. 316265, BIOCAPS) Ministerio de Ciencia y Tecnología (MAT2010-18281) and the Universidad de Vigo (64902). The technical staff of CACTI (University of Vigo) is gratefully acknowledged.

References

1. J. Breme, V. Biehl, *Handbook of Biomaterials Properties* (Chapman & Hall, London, 1998)
2. D.M. Brunette, P. Tengvall, M. Textor, P. Thomsen, *Titanium in Medicine: Material Science, Surface Science, Engineering, Biological Responses and Medical Applications* (Springer, New York, 2001)
3. B.D. Boyan, D.D. Dean, C.H. Lohmann, D.L. Cochran, V.L. Sylvia, Z. Schwartz, *The Titanium Bone-Cell Interface In Vitro. The Role of the Surface in Promoting Osseointegration* (Springer, Berlin, 2001)
4. P.M. Burgos, L. Rasmusson, L. Meirelles, L. Sennerby, *Clin. Implant Dent. Relat. Res.* **10**, 181 (2008)
5. S.A. Cho, S.K. Jung, *Biomaterials* **24**, 4859 (2003)
6. A. Gupta, *Internet J. Dent. Sci.* **2009**, 7 (2009)
7. M.H. Hong, S.M. Huang, B.S. Luk'yanchuk, T.C. Chong, *Sens. Actuators A-Phys.* **108**, 69–74 (2003)
8. A. Kurella, N.B. Dahotre, *J. Biomater. Appl.* **20**(1), 5–50 (2005)
9. L. Calcagnile, M.G. Grimaldi, P. Baeri, *J. Appl. Phys.* **76**(3), 1833 (1994)
10. Z. Chvoj, V. Cháb, O. Borusik, *Thermo-Chem. Acta* 280–281, 261 (1996)
11. D. Klinger, J. Auleytner, D. Zymierska, *Cryst. Res. Technol.* **32**(7), 983 (1997)
12. I.V. Grozescu, W.M.M. Yunus, M.M. Moxin, *J. Phys. D Appl. Phys.* **33**, 677 (2000)
13. J.C. Conde, Thesis Dissertation, University of Vigo (2004). ISBN 84-8158-320-0
14. H.E. Götz, M. Müller, A. Emmel, U. Holzwarth, R.G. Erben, R. Stangl, *Biomaterials* **25**, 4057 (2004)
15. M. Müller, F.F. Hennig, T. Hothorn, R. Stangl, *J. Biomech.* **39**, 2123 (2006)
16. J. Li, H. Liao, B. Fartash, L. Hermansson, T. Johnsson, *Biomaterials* **18**, 691 (1997)
17. J.C. Conde, F. Lusquiños, P. González, J. Serra, B. León, L. Cultrera, D. Guido, A. Perrone, *Appl. Phys. A* **79**, 1105 (2004)
18. J.C. Conde, P. González, F. Lusquiños, S. Chiussi, J. Serra, B. León, *Appl. Surf. Sci.* **248**, 461 (2005)
19. J.C. Conde, E. Martín, S. Chiussi, F. Gontad, C. Serra, P. González: *Appl. Phys. Lett.* **97**, 014102-1 (2010)
20. ANSYS®, *HEAT TRANSFER, Analysis Guides and Others*, 1st edn. SAS IP, Inc.© (2009)
21. L. Ward, *The Constants of the Materials and Films*, 2nd edn. (IOP Publishing Ltd Institute of Physics, London, 1994)
22. M.W. Chase Jr, *NIST-JANAF Thermochemical Tables*, 4th edn. (The American Chemical Society and the American Institute of Physics, USA, 1998)
23. R.C. Weast, *Handbook of Chemistry and Physics* (CRC Press, Inc., USA, 1976)
24. M.W. Ribarsky, *Handbook of Optical Constant of Solids* (Academic Press, Inc., USA, 1985)
25. J. Tavakoli, M.E. Khosroshahi, M. Mahmoodi, *IJE Trans. B Appl.* **20**, 1 (2007)
26. M. Boivineau, C. Cagran, D. Doytier, V. Eyraud, M.-H. Nadal, B. Wilthan, G. Pottlacher, *Int. J. Thermophys.* **27**(2), 507 (2006)
27. J.J.Z. Li, W.L. Johnson, W.-K. Rhima, *Appl. Phys. Lett.* **89**, 111913 (2006)
28. J.C. Miller, R.F. Haglund (eds.), *Laser Ablation and Desorption* (Academic Press, USA, 1998)
29. H. Zhao, T. DebRoy, *J. Appl. Phys.* **93**, 10089–10096 (2003)
30. A. Kaplan, *J. Phys. D Appl. Phys.* **27**, 1805–1814 (1994)
31. C.J. Nonhof, *Material Processing with Nd-YAG lasers* (Scotland: Electrochemical, Ayz, 1988)
32. J. Greses, P.A. Hilton, C.Y. Barlow, W.M. Steen, *J. Laser Appl.* **16**, 9 (2004)